BNL-219912-2020-TECH

EIC-ADD-TN-009

High-frequency Impedance of Asymmetric Collimators for the EIC project

B. Podobedov

September 2020

Electron-Ion Collider

Brookhaven National Laboratory

U.S. Department of Energy

USDOE Office of Science (SC), Nuclear Physics (NP) (SC-26)

DISCLAIMER

High-frequency Impedance of Asymmetric Collimators for the EIC project

Boris Podobedov, Brookhaven National Laboratory, Upton, NY, USA

(Dated: September 30, 2020)

Abstract

The electron storage ring for the EIC project will require numerous beam collimators, expected to be the major contributors to the total impedance budget of the machine. The presently considered collimators are of the KEKB style, where a constant circular cross-section vacuum chamber is bent in the collimation plane towards the beam orbit and then brought back. In this note, the high frequency geometric impedance of these strongly asymmetric collimators is derived analytically by following the optical impedance formalism.

I. INTRODUCTION

The electron storage ring (ESR) for the EIC project [1] will require numerous beam collimators primarily to reduce the background detector noise. By design, these collimators are placed relatively close to the beam orbit, so they are expected to be the major contributors to the total impedance budget of the machine, especially in the transverse plane. Consequently, the impedance of these structures must be calculated with care because they may significantly affect collective beam dynamics at high current. A candidate collimator design presently being considered for the EIC is based on the movable mask (collimator) design successfully implemented at KEKB [2]. Conceptually, this collimator consists of a constant circular cross-section vacuum chamber, which is bent, in the collimation plane, towards the beam orbit and then back, using two symmetric linear transitions, see Fig. 1. In spite of a circular pipe cross-section, from the point of view of geometric impedance this structure is not simple, because of its general 3D nature and a significant asymmetry in the collimation plane.

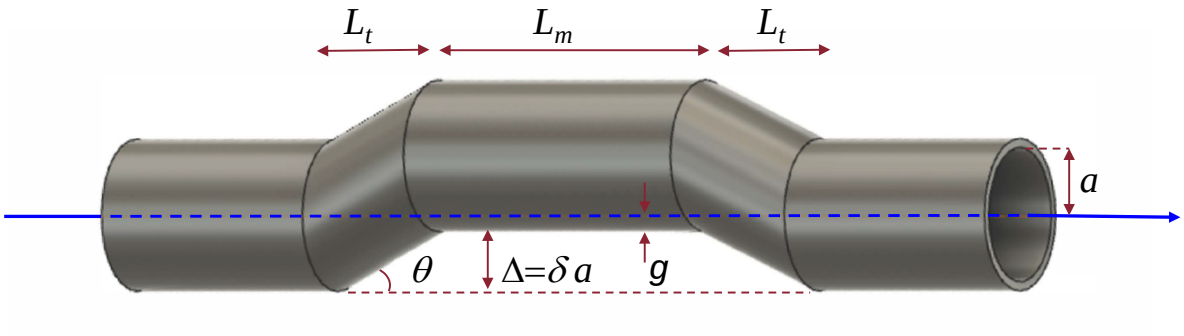

FIG. 1: KEKB-style asymmetric collimator geometry. All straight pipes have a circular cross-section with radius a. The middle pipe is displaced vertically by $\Delta = \delta\, a < a$. The nominal beam trajectory is centered in the incoming and outgoing pipes, and is distance $g = (1-\delta)a$ away from the nearest wall of the middle pipe. The length of the middle section is L_m. The transitions are length L_t each, making the tapering angle $\theta = \arctan(\Delta/L_t)$.

While the geometric impedance for this and other vacuum chamber components of the EIC ESR is being primarily calculated with time-domain EM field solver codes, having an analytical model for the impedance is extremely valuable, especially at high frequencies. This allows one to benchmark the codes against theory in the most demanding regime,

especially when calculating slowly-tapered 3D structures. On top of that, having the analytical impedance model at $\omega \to \infty$ allows one to rigorously determine the point-charge wake functions from the wake potentials provided by EM solvers, calculated with a relatively long bunch, see [3]-[4].

In the high frequency regime, the so-called optical model was developed [5, 6] which gives the impedance of collimator-like structures, i.e. the ones with the minimum aperture smaller than that of the incoming or outgoing pipes (or both). The power of the model and the method used to calculate it, derived in [5, 6], is that the impedance of complicated 3D structures is calculated from 2D solutions of Poisson's equation. These solutions are only needed for the incoming and/or outgoing pipe cross-sections as well as at the minimum cross-section of the structure; the details of the cross-sectional variation along the collimator transitions do not matter.

The EIC collimator geometry is not completely defined this early in the design stage. Detailed studies of the impedance dependence on geometric parameters (as well as the impedance implications for collective beam dynamics) are on-going. In this note we will derive the expressions for the longitudinal and transverse impedance, limiting the latter to the collimation plane only. We will then study how these impedances depend on relevant geometric parameters. We will also present the impedance values for what is presently called the "nominal" parameter case, specifically a=25 mm, $\delta = \Delta/a$=0.6 and the beam orbit centered in the incoming and outgoing pipes, see Fig. 1.

Through the rest of the note we will assume that the collimation is performed in the vertical plane, such as depicted in the figure, and we will denote the corresponding vertical impedance by $Z_\perp$. Of course, the results would apply equally well for the collimation in the horizontal plane.

We will use Gaussian units in this note. Conversion to SI can be accomplished by multiplying the impedance expressions by $Z_0 c/(4\pi)$, where $Z_0 = 377\,\Omega$ is the free space impedance.

The rest of this note is organized as follows. In Section II we review the most essential aspects of the optical impedance model, that are necessary for understanding the rest of the note. We also present some key expressions needed for the impedance calculation. In Section III we derive the longitudinal and transverse impedance expressions for the asymmetric collimator geometry. In Section IV we discuss the impedance dependence on key parameters, as well as other physics aspects. Finally, in Section V we summarize our results and outline

some of the implications for the EIC ESR.

II. OPTICAL IMPEDANCE MODEL BASICS [5, 6]

Optical impedance model applies at high frequencies, where the beam-induced EM wave propagation can be approximated by the laws of geometric optics, i.e. diffraction effects could be neglected. Two conditions are necessary for the model to be applicable. First, the frequency must be high, $\omega \gg c/g$, where g is the minimum aperture of the structure. If the structure is tapered, it is further required that $\omega \gg c/(g\theta)$, with θ being the tapering angle. The second condition is that the structure length L must be short compared to the catch-up distance, $L \ll l$, where the catch-up distance is defined, as usual, by $l = g^2\omega/c$.

Some long collimator structures, with $L \gg l$, could also be treated by means of the optical impedance model. This case, however, requires that they have a constant minimum cross-section pipe much longer than l, while the transition lengths at the entrance and the exit of the structure are each much shorter than l. The total impedance of such long collimator is simply given by the sum of the optical model impedances due to the entrance and exit transitions.

In the optical regime the longitudinal impedance $Z_\parallel$ is purely real and independent of frequency. The transverse impedance $Z_\perp$ is also real and scales as $1/\omega$. If the outgoing pipe cross-section coincides with the minimum aperture, the structure is called a step-in. The optical model impedance of a step-in is zero. Conversely, the impedance of a step-out structure (the one with the incoming pipe cross-section matching the minimum aperture) as well as the impedance of a general structure with the minimum aperture different from that of the the incoming and outgoing pipes is not zero.

As shown in [5, 6], the longitudinal impedance on the reference trajectory (i.e. at $x = y = 0$), is given by

$$Z_\parallel = \frac{1}{2\pi c}\left[\int_{S_B} (\nabla\phi_{m,B})^2\, dS - \int_{S_{ap}} \nabla\phi_{m,A}\cdot\nabla\phi_{m,B}\, dS \right], \tag{1}$$

where the first integral is performed over the cross-section of the outgoing pipe (denoted by B), and the second integral is over the aperture cross-section, see Fig. 2. Here the potential $\phi_{m,A}$ is the solution to Poisson's equation

$$\nabla^2\phi_{m,A} = -4\pi\delta(y)\delta(x), \tag{2}$$

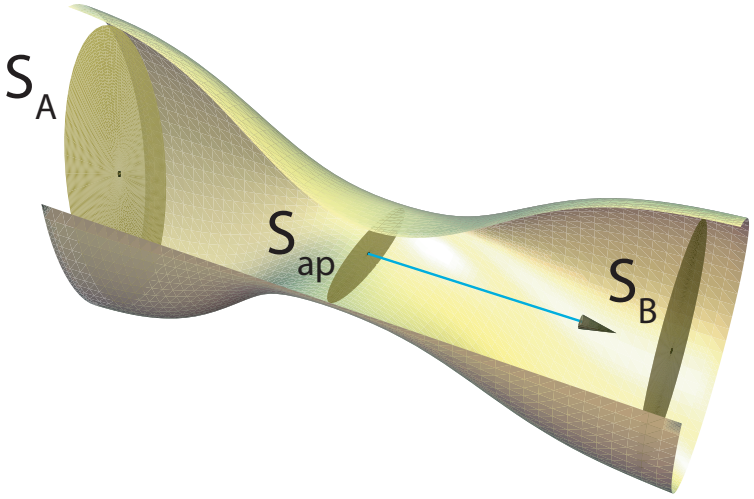

FIG. 2: Sketch (taken, by permission, from [5]) of a generalized 3D transition, showing the regions A, aperture, and B, with cross sections S_A, S_{ap}, and S_B, respectively. Beam pipe cross-sections upstream of A (incoming pipe) and downstream of B (outgoing pipe) are constant.

with the boundary condition $\phi_{m,A} = 0$ on metallic boundary C_A that encloses S_A. Similar equations hold for $\phi_{m,B}$ in region B. By applying Green's first identity the surface integrals in Eq. (1) can be reduced to a line integral

$$Z_{\parallel} = -\frac{1}{2\pi c} \int_{C_{ap}} \phi_{m,B}\, \mathbf{n} \cdot \nabla \phi_{m,A}\, dl, \tag{3}$$

where C_{ap} is the contour enclosing the aperture with its unit normal vector $\mathbf{n}$ directed outwards.

For axially asymmetric structures, assuming, for simplicity, a symmetry plane in x, but not y, the transverse impedance is conventionally represented as [7],

$$\begin{aligned} Z^x_{\perp,tot} &= x_1 Z^x_{\perp,d} - x_2 Z_{\perp,q}, \\ Z^y_{\perp,tot} &= Z^y_{\perp,m} + y_1 Z^y_{\perp,d} + y_2 Z_{\perp,q}, \end{aligned} \tag{4}$$

where x_1, y_1, x_2 and y_2 stand, respectively, for the offsets of the leading and trailing particles with respect to the reference trajectory; all offsets are assumed to be small. $Z^y_{\perp,m}$ denotes the vertical monopole impedance component, which results in the kick to the 2nd particle[1],

[1] Beam particles are assumed ultra-relativistic, so, from causality, the leading particle experiences no kick.

which is independent of all transverse offsets. The monopole component is only present if there is no symmetry in the corresponding plane, which applies to the vertical plane for the orientation of the KEKB-style collimator shown in Fig. 1. In Eq. (4), $Z^x_{\perp,d}$ and $Z^y_{\perp,d}$ stand for the dipole impedance components in the corresponding planes, and the quadrupole impedance component, $Z_{\perp,q}$, has the same magnitude in both planes but it comes in with the opposite signs.

As was mentioned in the Introduction, in this note we will concentrate on finding the impedance in the collimation plane only. Therefore, the super-script y will be omitted below and $Z_{\perp,m}$, $Z_{\perp,d}$, and $Z_{\perp,q}$ will denote the respective vertical impedance components.

The optical model expressions for all transverse impedance components can be cast into a form similar to Eq. (3)[2],

$$Z_{\perp,m} = -\frac{1}{2\pi\omega}\int_{C_{ap}} \phi_{d,B}\ \mathbf{n}\cdot\nabla\phi_{m,A}\, dl, \tag{5}$$

$$Z_{\perp,d} = -\frac{1}{2\pi\omega}\int_{C_{ap}} \phi_{d,B}\ \mathbf{n}\cdot\nabla\phi_{d,A}\, dl, \tag{6}$$

$$Z_{\perp,q} = -\frac{1}{\pi\omega}\int_{C_{ap}} \phi_{m,B}\ \mathbf{n}\cdot\nabla\phi_{q,A}\, dl, \tag{7}$$

where the potentials $\phi_{d,A}$ and $\phi_{q,A}$ are the solutions to Poisson's equations

$$\nabla^2\phi_{d,A} = -4\pi\delta'(y)\delta(x), \tag{8}$$

$$\nabla^2\phi_{q,A} = -2\pi\delta''(y)\delta(x), \tag{9}$$

with respective boundary conditions $\phi_{d,A} = 0$ and $\phi_{q,A} = 0$ on metallic boundary C_A that encloses S_A. Similar equations hold for $\phi_{d,B}$ and $\phi_{q,B}$ in region B.

The potentials in the region of interest can be found from the Green function solution to

$$\nabla^2 G(x,y,y_0) = -4\pi\delta(x)\delta(y-y_0), \tag{10}$$

with the boundary condition $G = 0$ on metallic boundary that encloses the region of interest.

[2] Only Eq. (5) appears explicitly in [5, 6], see i.e. Eq. (51) of [6]. We derived Eqs. (6) and (7) in a similar manner starting from the corresponding expressions in the surface integral form (i.e. similar to Eq. (1) of this note) which appear in [5, 6].

Here the source particle is located at $x = 0$, $y = y_0$. The potentials are given by

$$\phi_m(x, y) = [G(x, y, y_0)]_{y_0=0}, \tag{11}$$

$$\phi_d(x, y) = \left[\frac{\partial}{\partial y_0} G(x, y, y_0)\right]_{y_0=0}, \tag{12}$$

$$\phi_q(x, y) = \frac{1}{2}\left[\frac{\partial^2}{\partial y_0^2} G(x, y, y_0)\right]_{y_0=0}. \tag{13}$$

To summarize, if we know the 2D potentials in the incoming (A) and outgoing (B) pipes of a collimator-like structure then Eq. (3) and Eqs. (5)-(7) give, respectively, the longitudinal and the transverse optical model impedances for this structure. Obviously, if the structure is an iris, i.e. the incoming and outgoing pipes have the same cross-section, only one set of potentials is required to find the impedance.

To find the optical impedance model for a long collimator, as defined in the beginning of this section, the potential in the minimum cross-section is also required. In this case, the impedance of the entrance transition is calculated as above, by taking the middle section to be the "outgoing pipe" B. Similarly, the exit transition impedance is calculated by taking the middle section to be the "incoming pipe" A. The total impedance of the structure is then simply the sum of the entrance and exit transition impedances.

We end this section with one important aspect, not emphasized in [5, 6]. If the frequency is taken to be high enough, the catch-up distance becomes longer than the length of any collimator-like structure. Therefore, at high frequency, all collimator-like structures are equivalent to irises as far as their high frequency impedance goes. In other words, their asymptotic high frequency impedance is given by the optical model for the iris-like structure with the same aperture as the original collimator.

III. IMPEDANCE DERIVATION FOR ASYMMETRIC COLLIMATOR

As follows from the previous section, for the KEKB-style collimator of any length, depicted in Fig. 1, the high frequency optical impedance model, $\lim_{\omega\to\infty} Z(\omega)$, denoted Z^∞ below, will be the same as for the equivalent iris (index ir below), shown in Fig. 3,

$$\begin{aligned} Z_\parallel^\infty &= Z_\parallel^{ir}, \\ Z_\perp^\infty &= Z_\perp^{ir}. \end{aligned} \tag{14}$$

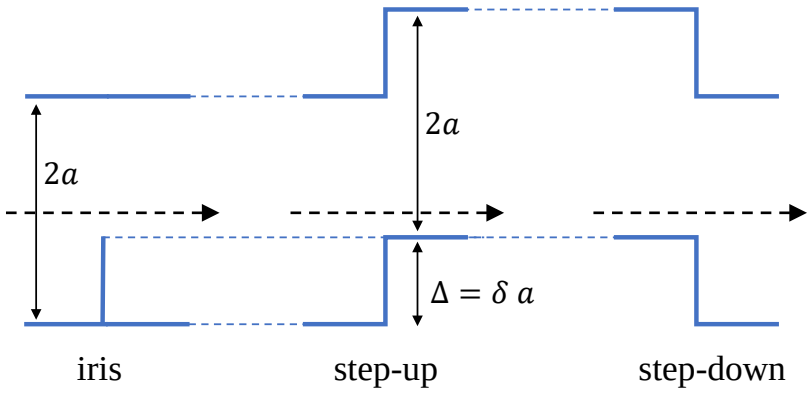

FIG. 3: Lateral view of the iris, step-up and step-down. All straight pipes have a circular cross-section with radius a. The nominal beam trajectory (dashed arrow) is centered in the incoming pipe for the step-up, in the outgoing pipe for the step-down and in both pipes for the iris.

For long collimators, there will also be an intermediate range of high frequencies, where their optical impedance model, Z^{long}, is given by the sum of the impedances due to the step-up (su) and step-down (sd) transitions, also shown in Fig. 3,

$$\begin{aligned} Z_{\parallel}^{long} &= Z_{\parallel}^{su} + Z_{\parallel}^{sd}, \\ Z_{\perp}^{long} &= Z_{\perp}^{su} + Z_{\perp}^{sd}. \end{aligned} \tag{15}$$

To find both models, we therefore need to find the optical impedances of the iris, step-up, and step-down transitions. We emphasize that none of them can be considered a step-in (or a step-out) and therefore all are expected to result in non-zero impedance, except for some limiting cases, i.e. when δ=0 (straight pipe). Below we outline the optical model impedance derivation for these three structures.

Green's function for a vertically displaced beam in a circular pipe is given by

$$G(x,y,y_0) = \log\left(\frac{y_0^2}{a^2}\right) - \log\left(\frac{x^2+(y-y_0)^2}{\left(y-\frac{a^2}{y_0}\right)^2+x^2}\right). \tag{16}$$

This equation can be easily obtained, for instance, by the method of images.

Substituting Eq. (16) into Eqs. (11)-(13) we obtain the potentials for the regions where the orbit is centered in the pipe, specifically the incoming pipe of the step-up, the outgoing

pipe of the step-down, and for both pipes of the iris,

$$\phi_m(x,y) = -\log\left(\frac{x^2+y^2}{a^2}\right), \tag{17}$$

$$\phi_d(x,y) = -\frac{2y\left(-a^2+x^2+y^2\right)}{a^2\left(x^2+y^2\right)}, \tag{18}$$

$$\phi_q(x,y) = x^2\left(\frac{2}{a^4} - \frac{2}{\left(x^2+y^2\right)^2}\right) - \frac{x^2+y^2}{a^4} + \frac{1}{x^2+y^2}. \tag{19}$$

For the regions with off-centered beam, i.e. the outgoing pipe of the step-up and the incoming pipe of the step-down, the potentials are obtained similarly, except in Eqs. (11)-(13) y is replaced by $y-\Delta$ and "$y_0 = 0$" condition is replaced by "$y_0 = -\Delta$". This results in

$$\phi_m(x,y) = \log\left(\frac{\Delta^2}{a^2}\right) - \log\left(\frac{x^2+y^2}{\left(\frac{a^2}{\Delta} - \Delta + y\right)^2 + x^2}\right), \tag{20}$$

$$\phi_d(x,y) = \frac{2y}{x^2+y^2} - \frac{2\left(-a^2\Delta + a^2y + \Delta^3 + \Delta x^2 + \Delta y^2 - 2\Delta^2 y\right)}{a^4 - 2a^2\Delta^2 + 2a^2\Delta y + \Delta^4 + \Delta^2x^2 + \Delta^2y^2 - 2\Delta^3 y}, \tag{21}$$

$$\begin{aligned}\phi_q(x,y) =& \frac{2a^4x^2}{\left(a^4 + 2a^2\Delta(y-\Delta) + \Delta^2\left(x^2 + (y-\Delta)^2\right)\right)^2} \\ &- \frac{x^2 + (y-\Delta)^2}{a^4 + 2a^2\Delta(y-\Delta) + \Delta^2\left(x^2 + (y-\Delta)^2\right)} + \frac{y^2-x^2}{\left(x^2+y^2\right)^2}.\end{aligned} \tag{22}$$

We now proceed to discuss the integration path in Eqs.(3) and (5)-(7). The aperture region for the iris, step-up and step-down is sketched in Fig. 4. Contour C_{ap} encloses the entire cross-section of the aperture S_{ap}. However, for the iris and step-down, only the bottom part of C_{ap} contributes to the integrals in Eqs.(3) and (5)-(7). This is due to the zero boundary condition for all the region B potentials at the top part of C_{ap}. Conversely, for the step-up, the contribution to the impedance only comes from the top part of the contour. Because all three structures are horizontally symmetric (and so are the potentials), the integrals can be further restricted to the region of positive x and then doubled.

The normal vector in Eqs.(3) and (5)-(7)is given by

$$\mathbf{n} = \left(\frac{x}{a}, \pm\sqrt{1 - \frac{x^2}{a^2}}\right), \tag{23}$$

with +/- corresponding to the top/bottom parts of the contour.

After plugging the appropriate potentials from Eqs. (17)-(19) and Eqs. (20)-(22) into Eqs.(3) and (5)-(7), then selecting the integration path and the corresponding normal vector

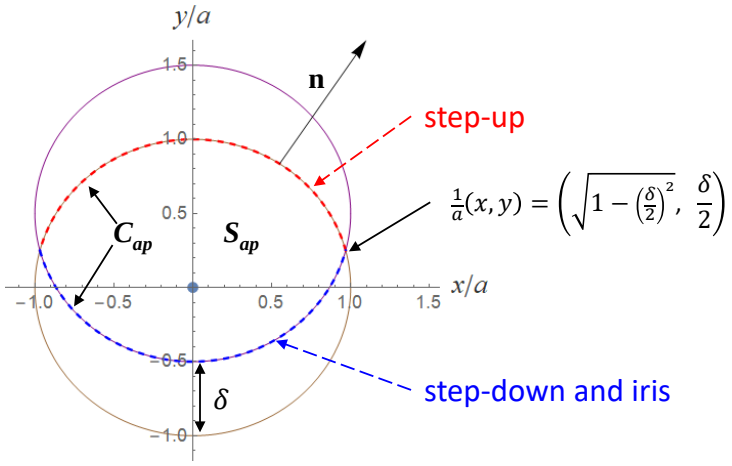

FIG. 4: Integration path explanation. Aperture S_{ap} is enclosed by contour C_{ap}, shown in dash. Parts of the contour that contribute to the integrals in Eqs.(3) and (5)-(7) for the respective structures are marked by dashed arrows. Also shown is the normal vector $\mathbf{n}$, given by Eq. (23).

as described above, and, finally, switching the integration variable to the compliment of the polar angle[3], $\alpha = \sin^{-1}(x/a)$, we get the final impedance expressions. They are, for the iris,

$$Z_{\parallel}^{ir} = \frac{2}{\pi c}\int_0^{\beta} \frac{(-1+\delta\cos(\alpha))\log\left(1+\delta^2-2\delta\cos(\alpha)\right)}{1+\delta^2-2\delta\cos(\alpha)}\,d\alpha, \tag{24}$$

$$Z_{\perp,m}^{ir} = -\frac{4}{\pi\omega a}\int_0^{\beta} \frac{\delta(\delta-2\cos(\alpha))(\delta-\cos(\alpha))(1-\delta\cos(\alpha))}{\left(1+\delta^2-2\delta\cos(\alpha)\right)^2}\,d\alpha, \tag{25}$$

$$\begin{aligned} Z_{\perp,d}^{ir} = &\frac{4}{\pi\omega a^2}\int_0^{\beta} \frac{\delta(\delta-2\cos(\alpha))(\delta-\cos(\alpha))}{\left(1+\delta^2-2\delta\cos(\alpha)\right)^3} \\ &\times\left(\left(2+6\delta^2+\delta^4\right)\cos(\alpha)+\delta\left(-2\left(2+\delta^2+\left(1+\delta^2\right)\cos(2\alpha)\right)+\delta\cos(3\alpha)\right)\right)\,d\alpha, \end{aligned} \tag{26}$$

$$\begin{aligned} Z_{\perp,q}^{ir} = &\frac{4}{\pi\omega a^2}\int_0^{\beta} \log\left(1+\delta^2-2\delta\cos(\alpha)\right) \\ &\times\left(-1+\delta\cos(\alpha)-\frac{3\delta^2-\delta\left(3+\delta^2\right)\cos(\alpha)+\cos(2\alpha)}{\left(1+\delta^2-2\delta\cos(\alpha)\right)^3}+2\sin^2(\alpha)\right)\,d\alpha, \end{aligned} \tag{27}$$

[3] For the step-up, due to angular-independent integration path, the entire derivation is easier in polar coordinates.

for the step-up,

$$Z_{\parallel}^{su} = \frac{2}{\pi c}\int_0^{\beta} \log\left(1-\delta^2+\delta^4-2\delta\left(-1+\delta^2\right)\cos(\alpha)\right)\, d\alpha, \tag{28}$$

$$Z_{\perp,m}^{su} = \frac{-4}{\pi\omega a}\int_0^{\beta} \frac{\delta\left(1-2\delta^2+(\delta+\delta^3)\cos(\alpha)-(-1+\delta^2)\cos(2\alpha)\right)}{-1+\delta^2-\delta^4+2\delta\left(-1+\delta^2\right)\cos(\alpha)}\, d\alpha, \tag{29}$$

$$Z_{\perp,d}^{su} = \frac{-8}{\pi\omega a^2}\int_0^{\beta} \frac{\delta(\delta-2\cos(\alpha))\cos(\alpha)\left(-\delta+(-1+\delta^2)\cos(\alpha)\right)}{-1+\delta^2-\delta^4+2\delta\left(-1+\delta^2\right)\cos(\alpha)}\, d\alpha, \tag{30}$$

$$Z_{\perp,q}^{su} = \frac{8}{\pi\omega a^2}\int_0^{\beta} \cos(2\alpha)\log\left(1-\delta^2+\delta^4-2\delta\left(-1+\delta^2\right)\cos(\alpha)\right)\, d\alpha, \tag{31}$$

and for the step-down,

$$Z_{\parallel}^{sd} = \frac{2}{\pi c}\int_0^{\beta} \frac{\left(-1+\delta^2\right)\log\left(1+\delta^2-2\delta\cos(\alpha)\right)}{1+\delta^2-2\delta\cos(\alpha)}\, d\alpha, \tag{32}$$

$$Z_{\perp,m}^{sd} = \frac{4}{\pi\omega a}\int_0^{\beta} \frac{\delta\left(-1+\delta^2\right)\left(1+\delta^2-3\delta\cos(\alpha)+\cos(2\alpha)\right)}{\left(1+\delta^2-2\delta\cos(\alpha)\right)^2}\, d\alpha, \tag{33}$$

$$Z_{\perp,d}^{sd} = \frac{8}{\pi\omega a^2}\int_0^{\beta} \frac{\delta(\delta-2\cos(\alpha))(\delta-\cos(\alpha))\left(-2\delta+(1+\delta^2)\cos(\alpha)\right)}{\left(1+\delta^2-2\delta\cos(\alpha)\right)^3}\, d\alpha, \tag{34}$$

$$Z_{\perp,q}^{sd} = \frac{-8}{\pi\omega a^2}\int_0^{\beta} \frac{\left(3\delta^2-\delta\left(3+\delta^2\right)\cos(\alpha)+\cos(2\alpha)\right)\log\left(1+\delta^2-2\delta\cos(\alpha)\right)}{\left(1+\delta^2-2\delta\cos(\alpha)\right)^3}\, d\alpha, \tag{35}$$

where the upper integration limit is $\beta = \arccos(\delta/2)$, and $0 \le \delta < 1$ is assumed for all expressions. As explained earlier, the impedance expressions for the iris also give the high frequency optical model for a collimator structure of arbitrary length, while the expressions for the step-up and step-down together give the intermediate frequency range optical model for long collimators, see Eqs. (14) and (15).

As presented, the impedance expressions are valid for $0 \le \delta < 1$, corresponding to the upward displacement of the collimator middle pipe. It can be shown that, as expected, $Z_{\perp,m}$ is an odd function of δ. It is negative for $\delta > 0$ for the iris and step-down, and positive for the step-up, which corresponds to the monopole wakefield kick towards (away for the step-up) the closest wall of the collimator middle pipe. All other impedances are positive and even functions of δ, corresponding to the energy loss and defocusing wakefield kicks, all independent of the direction of the middle pipe displacement. Mathematically, the impedance symmetry relations with respect to δ appear because, for each structure, the

parts of C_{ap} that contribute or not contribute to the integrals in Eqs.(3) and (5)-(7), as specified above for $\delta > 0$, switch places for $\delta < 0$.

With the exception of the longitudinal impedance, all other impedances could be expressed in closed-form. However, the resulting expressions come out to be less compact, so we decided to leave all of the equations (24)-(35) in the integral form. Fortunately, the integrals they contain are well-behaved and they can be easily evaluated, i.e. in Mathematica.

IV. DISCUSSION

A. Extreme cases

It is convenient to first discuss the two extreme cases, the limit of straight pipe, $\delta \to 0$, as well as the limit of "extreme collimation", $\delta \to 1$, when the nominal beam orbit is close to the wall of the collimator middle section.

As expected, all impedance expressions linearly go to zero in the limit of straight pipe, $\delta \to 0$. For all geometries, the corresponding impedance slopes with δ are the same, except for the sign change for $Z^{su}_{\perp,m}$, specifically,

$$\lim_{\delta\to+0} \frac{\partial}{\partial\delta} Z^{ir}_{\parallel} = \lim_{\delta\to+0} \frac{\partial}{\partial\delta} Z^{su}_{\parallel} = \lim_{\delta\to+0} \frac{\partial}{\partial\delta} Z^{sd}_{\parallel} = \frac{4}{\pi c}, \tag{36}$$

$$\lim_{\delta\to0} \frac{\partial}{\partial\delta} Z^{ir}_{\perp,m} = -\lim_{\delta\to0} \frac{\partial}{\partial\delta} Z^{su}_{\perp,m} = \lim_{\delta\to0} \frac{\partial}{\partial\delta} Z^{sd}_{\perp,m} = -\frac{2}{\omega a}, \tag{37}$$

$$\lim_{\delta\to+0} \frac{\partial}{\partial\delta} Z^{ir}_{\perp,d} = \lim_{\delta\to+0} \frac{\partial}{\partial\delta} Z^{su}_{\perp,d} = \lim_{\delta\to+0} \frac{\partial}{\partial\delta} Z^{sd}_{\perp,d} = \frac{32}{3\pi\omega a^2}, \tag{38}$$

$$\lim_{\delta\to+0} \frac{\partial}{\partial\delta} Z^{ir}_{\perp,q} = \lim_{\delta\to+0} \frac{\partial}{\partial\delta} Z^{su}_{\perp,q} = \lim_{\delta\to+0} \frac{\partial}{\partial\delta} Z^{sd}_{\perp,q} = \frac{16}{3\pi\omega a^2}. \tag{39}$$

Linear relations of the impedances to δ, based on these slopes, hold approximately for $\delta \ll 1$.

For the step-up, $Z^{su}_{\parallel}$ and $Z^{su}_{\perp,q}$ also go to zero in the opposite limit, $\delta \to 1$. For this geometry, this could be argued to be similar to the case of a step-in, which has zero impedance in the optical model. Note, however, that the step-in analogy is imperfect, because the transverse monopole and dipole impedances of the step-up remain non-zero when $\delta \to 1$.

For the step-down and iris, in the limit of $\delta \to 1$, all impedances go to infinity (negative for the monopole case). Expressed in terms of $g = (1-\delta)a$, i.e. the shortest beam distance to the edge of the iris or to the incoming pipe wall of the step-down, these divergences are logarithmic for the longitudinal impedance. For the transverse impedance, they scale as the

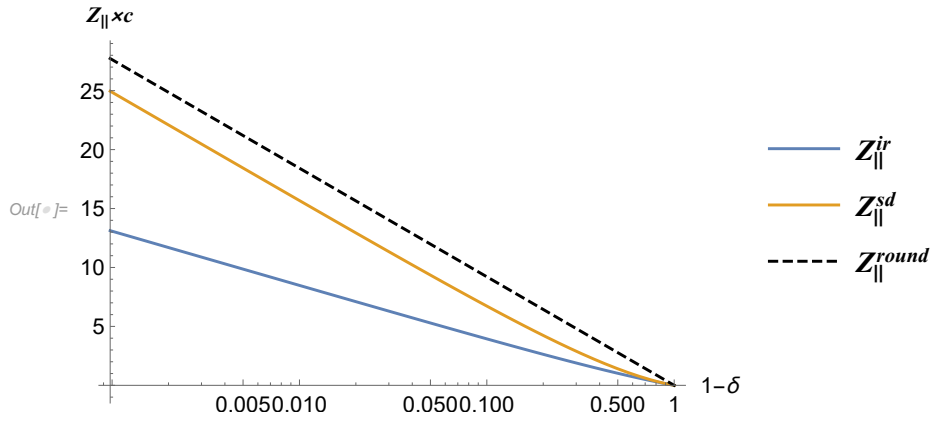

FIG. 5: Longitudinal impedance for the iris and step-down as a function of normalized beam distance to the edge of the iris or closest wall. Impedance of axially-symmetric iris is shown in black dash.

inverse power of distance for the monopole, and the inverse 2nd power of distance in case of dipole or quadrupole. These scalings are illustrated in Figs. 5, 6 and 7.

The figures also include, in black dash, the impedance of an axially symmetric iris of aperture $b = g = (1-\delta)a$, centered in a pipe of radius a, as well as the impedance of axially symmetric step-out of equal radial dimensions. The longitudinal impedance is the same for both cases, and it is denoted by $Z_\parallel^{round}$; a more specific super-script is used for two (different) transverse impedances. The impedance expressions are ([8], [9], [10])

$$Z_\parallel^{round} = \frac{4}{c}\log(a/b) = -\frac{4}{c}\log(1-\delta), \tag{40}$$

$$Z_\perp^{round\ iris} = \frac{2}{\omega b^2}\left(1-\frac{b^4}{a^4}\right) = \frac{2}{\omega(1-\delta)^2a^2}(1-(1-\delta)^4), \tag{41}$$

$$Z_\perp^{round\ step-out} = \frac{4}{\omega b^2}\left(1-\frac{b^2}{a^2}\right) = \frac{4}{\omega(1-\delta)^2a^2}(1-(1-\delta)^2). \tag{42}$$

(For axially symmetric geometry the total transverse impedance kick is independent of the displacement of the trailing charge, therefore $Z_\perp^{round}$ is purely dipolar, while the monopole and quadrupole impedance components are both zero.)

As is clear from Fig. 5, the linear slopes (in log-linear scale) for small distances indicate logarithmic divergence of longitudinal impedance when $\delta \to 1$. Furthermore, in this limit, the longitudinal impedance of the (asymmetric) iris is slightly less than half of the axially symmetric one. The impedance of the step-down for $\delta \to 1$ is slightly less than the impedance of the axially symmetric iris.

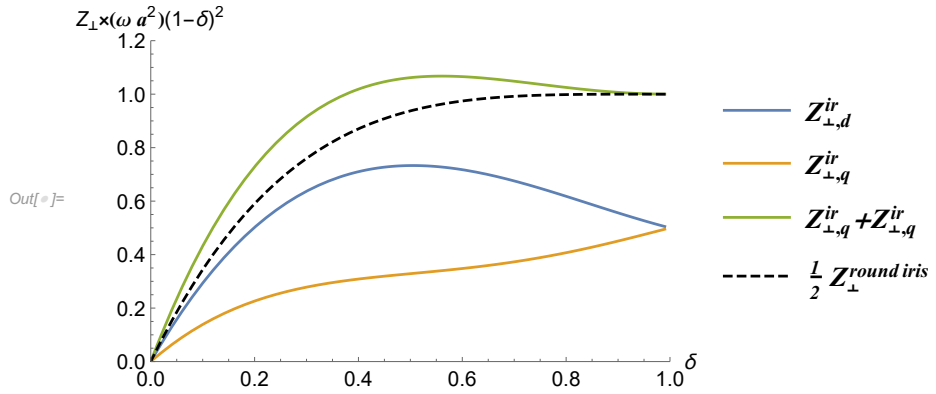

FIG. 6: Dipole and quadrupole impedances for the iris and their sum, all multiplied by $(\omega a^2)(1-\delta)^2$ (solid curves). Also plotted is one half of the impedance of the axially-symmetric iris, multiplied by the same factor (black dashed curve).

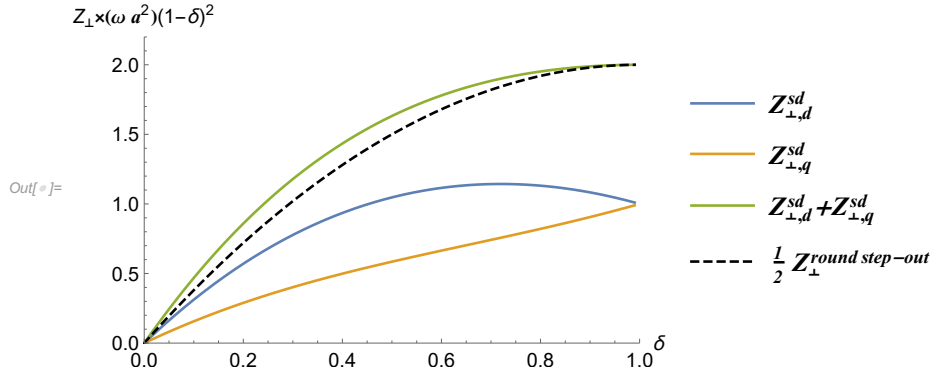

FIG. 7: Dipole and quadrupole impedances for the step-down, multiplied by $(\omega a^2)(1-\delta)^2$, and their sum (solid curves). Also plotted is one half of the impedance of the axially-symmetric step-out, multiplied by the same factor (black dashed curve).

Figure 6 illustrates that close to the edge of the iris, the dipole and quadrupole transverse impedance components, both diverging as $(1-\delta)^{-2}$, become equal. This is intuitively clear, because for close-to-the-edge case, the edge curvature should not matter, so this becomes equivalent to a planar geometry with transnational symmetry in the horizontal plane. In this case, the total horizontal kick experienced by the beam, proportional to $Z_{\perp,d}+(-Z_{\perp,q})$, must be zero, implying equal dipole and quadrupole impedances in the vertical plane, see Eq. (4). When added together, they make up exactly half the impedance of the axially symmetric iris, which is also expected because, in this limit, the (asymmetric) iris is single-sided.

Finally, Fig. 7 is the equivalent of Fig. 6 for the step-down transition, and it shows that similar conclusions also apply here. Note that the $\delta \to 1$ limit impedance values for the step-down are a factor of two higher than the equivalent ones for the (asymmetric) iris, which is expected from the ratio of the axially symmetric equivalents, Eqs. (41) and (42) in this limit.

B. Main Results

We now illustrate the main results of this note, Eqs. (24)-(35) plotting them separately for each geometry. For scale, we will also add the relevant axially symmetric results, from Eqs. (40)-(42).

In Fig. 8 we plot the impedance expressions for the iris, Eqs. (24)-(27). Due to different dimensions, the impedances are normalized, as shown in the legend, which makes all curves relatively close (i.e. for the same δ, all normalized impedances in the range shown are of the same order of magnitude). Due to factor of a difference in the normalizing coefficients between the monopole and dipole or quadrupole impedance components, this implies, as per Eq. (4), that for any reasonable off-axis displacement of particles, d, the monopole impedance kick is larger than the dipole or quadruple ones by a very big factor $\approx a/d$.[4]

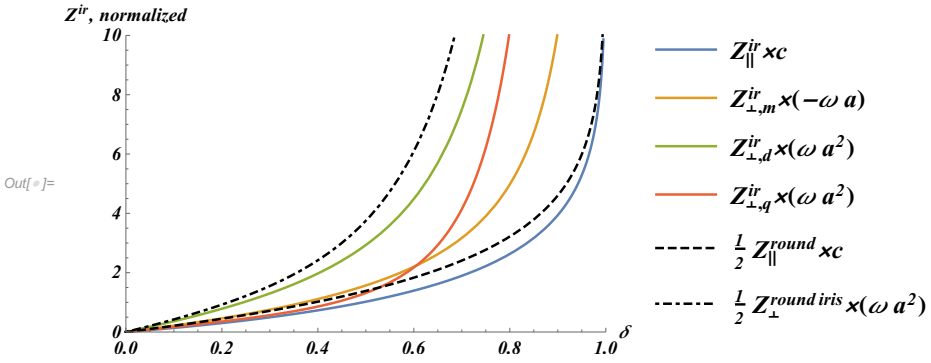

FIG. 8: Impedances for the iris, normalized as shown in the legend (solid curves). Also included, in dash and dot-dash, are equivalently normalized axially symmetric iris expressions, Eq. (40) and Eq. (41), each divided by 2.

[4] This factor reduces to $(1-\delta)a/d$ in the limit of $\delta \to 1$, discussed earlier.

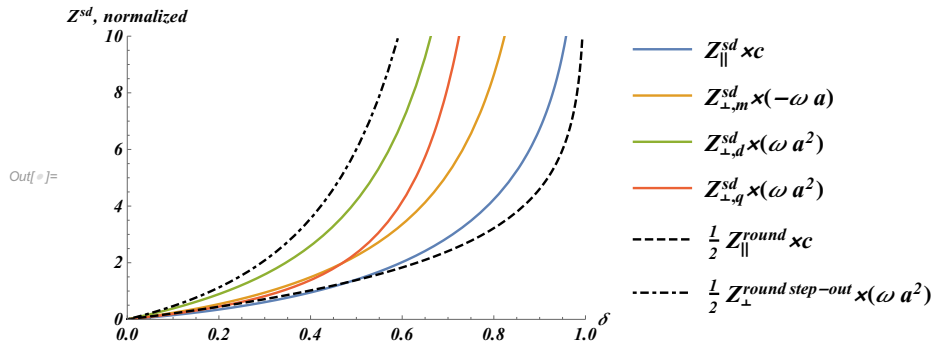

FIG. 9: Impedances for the step-down, normalized as shown in the legend (solid curves). Also included, in dash and dot-dash, are equivalently normalized axially symmetric step-out expressions, Eq. (40) and Eq. (42), each divided by 2.

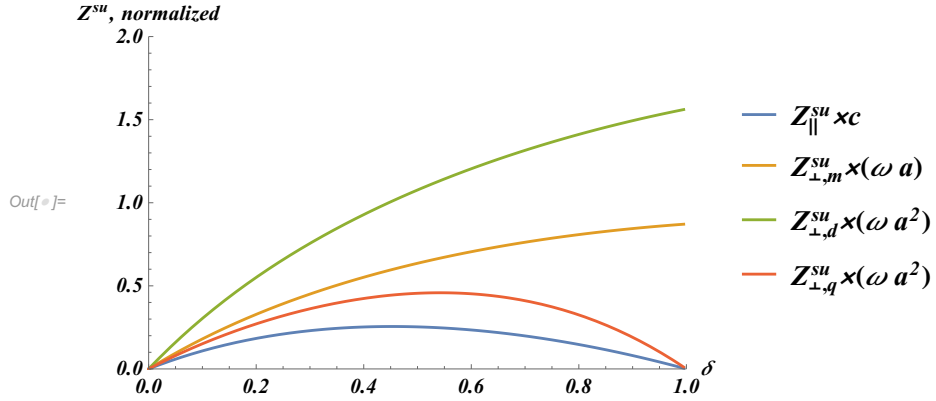

FIG. 10: Impedances for the step-up, normalized as shown in the legend.

In Fig. 9 we plot the impedance expressions for the step-down, Eqs. (32)-(35). While qualitatively similar, they are somewhat higher than the corresponding iris impedances, plotted above. In particular, for $\delta \gtrsim 0.5$, the longitudinal impedance, $Z^{sd}_{\parallel} > \frac{1}{2} Z^{round}_{\parallel}$, while for the iris $Z^{ir}_{\parallel} \leq \frac{1}{2} Z^{round}_{\parallel}$, for any value of δ.

Finally, Fig. 10 plots the impedance expressions for the step-up, Eqs. (28)-(31). Except when $\delta \ll 1$, where the corresponding impedances are approximately equal for all three geometries, the step-up impedances are noticeably smaller than those for the iris or the step-down. On top of that, as discussed in the previous sub-section, the step-up impedances do not diverge when $\delta \to 1$. Also, as mentioned previously, the monopole impedance is positive.

Comparing the figures in this sub-section, or going directly to the impedance expressions, it is easy to see that the impedance of the iris is always lower than the total impedance of the step-up and step-down, by approximately a factor of 2 over the entire range of δ. Because two non-interacting steps could be thought of as spread out infinitely far apart, this suggest that the collimator impedance is a fairly slow growing function of its length, L_m.

For easier comparison with numerical codes we also list the normalized impedance values calculated for the nominal case of $\delta = 0.6$:

$$Z_{\parallel}^{ir} \times c = 1.394, Z_{\perp,m}^{ir} \times (\omega a) = -2.199, Z_{\perp,d}^{ir} \times (\omega a^2) = 4.485, Z_{\perp,q}^{ir} \times (\omega a^2) = 2.175;$$
$$Z_{\parallel}^{su} \times c = 0.235, Z_{\perp,m}^{su} \times (\omega a) = 0.705, Z_{\perp,d}^{su} \times (\omega a^2) = 1.205, Z_{\perp,q}^{su} \times (\omega a^2) = 0.452;$$
$$Z_{\parallel}^{sd} \times c = 2.020, Z_{\perp,m}^{sd} \times (\omega a) = -3.353, Z_{\perp,d}^{sd} \times (\omega a^2) = 6.970, Z_{\perp,q}^{sd} \times (\omega a^2) = 4.153.$$

C. Off-center reference trajectories

As derived, the impedance expressions, Eqs. (24)-(35), are with respect to the reference trajectory that goes through the center of the incoming and outgoing pipes of the collimator. The expressions for the transverse impedances allow one to estimate the impedance for small deviations from the reference trajectory, as given by Eq. (4), however, how small these must be for a certain level of accuracy, is not immediately clear. The same applies to the longitudinal impedance expressions, which strictly assume that the beam travels on the reference trajectory. On the other hand, due to small denominators and/or divergent logarithmic terms in dipole and quadrupole impedances when δ approaches 1 (see i.e. Eqs.(26) and (27) for the iris), we expect significant sensitivity of the impedance to the reference trajectory for all three structures considered, and, by extension, for all significantly asymmetric transitions. The dependence of the impedances to the position of the reference trajectory is discussed below.

The derivation of Section III could be generalized for an arbitrary particle trajectory as long as it fits inside the structure, which requires that $-a \pm \Delta/2 < d - \Delta/2 < a \mp \Delta/2$, where d is the reference trajectory offset with respect to the center of the incoming pipe and the top sign corresponds to the case of $\Delta > 0$. Note that allowing for the trajectory displacement modifies the allowable range of Δ to $-1 + d < \Delta < 1 + d$ (or, equivalently, $-1 + d/a < \delta < 1 + d/a$).

We derived the impedances for the offset reference trajectory, and, as expected, the resulting expressions, identical to the original ones for $d = 0$, turned out to be significantly longer. We do not present these expressions here, but rather illustrate the impedance dependence in Fig. 11 using the longitudinal impedance for the iris as an example.

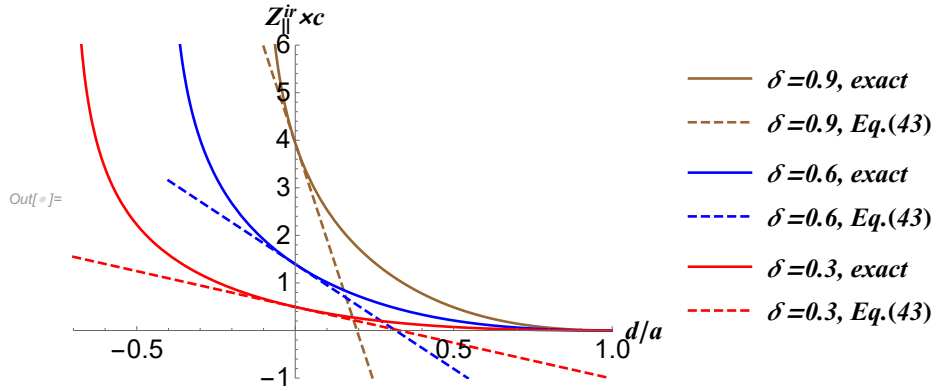

FIG. 11: Longitudinal impedance for the iris vs. the offset of the reference trajectory. Solid curves represent the results of the exact derivation, the dashed lines show the linear approximation given by Eq. (43).

Plotted in Fig. 11, for three representative values of parameter δ, are the results of the exact derivation for an arbitrary trajectory offset, and their linear (with the offset) approximations given by

$$Z_{\parallel}^{ir}(d) \approx Z_{\parallel}^{ir}(0) - \frac{4\delta}{1-\delta^2}\left(1 - \frac{\delta^2}{2} + \frac{4}{\pi}\left(1 - \frac{\delta^2}{4}\right)\sin^{-1}\left(\frac{\delta}{2}\right)\right)\frac{d}{a}, \tag{43}$$

where the impedance function argument explicitly shows the dependence on the offset of the reference trajectory y_{ref}. Specifically $Z_{\parallel}^{ir}(d) = Z_{\parallel}^{ir}(y_{ref} = d)$, and $Z_{\parallel}^{ir}(0)$ is identical to $Z_{\parallel}^{ir}$ of Eq. (24).

As expected, the impedance decreases monotonically with d, because the beam gets further from the iris. At the limit, $d \to a$, the impedance goes to zero, because the beam trajectory is close to the upper (smooth) wall of the pipe. For downward displacement of the reference trajectory the impedance diverges at $d/a = -1+\delta$, i.e. when the beam approaches the iris edge. For $\delta < 0.8$, the linear approximation, Eq. (43), gives less than 10% error when $|d/a| \lesssim 0.1$. As δ gets closer to 1, Eq. (43) remains valid in a progressively smaller range with respect to the d/a parameter, until the range becomes 0 at the limit of $\delta \to 1$.

For the transverse impedance components the dependence on the trajectory offset looks qualitatively similar to Fig. 11, except for the negative sign for $Z^{ir}_{\perp,m}$. We also point out that for the transverse impedances it holds in general that

$$Z_{\perp,m}(\tilde{d}) = Z_{\perp,m}(0) + \tilde{d}(Z_{\perp,d}(0) + Z_{\perp,q}(0)) + O[\tilde{d}]^2, \tag{44}$$

$$Z_{\perp,m}(0) = Z_{\perp,m}(\tilde{d}) - \tilde{d}(Z_{\perp,d}(\tilde{d}) + Z_{\perp,q}(\tilde{d})) + O[\tilde{d}]^2, \tag{45}$$

where the impedances are shown as the functions of the reference trajectory displacement. The equations simply mean that the total transverse kick on the trajectory displaced by $\tilde{d}$ or on the original trajectory (for simplicity taken to be zero) do not depend on which of the two trajectories is taken as the reference. These equations can be combined into the differential form, valid for arbitrary reference trajectory,

$$\left[\frac{\partial Z_{\perp,m}(y_{ref})}{\partial y_{ref}}\right]_{y_{ref}=d} = Z_{\perp,d}(d) + Z_{\perp,q}(d). \tag{46}$$

To the best of our knowledge, this monopole impedance property, which must be valid for all frequency ranges and all impedance-carrying structures, has not been pointed out before. Equation (46) can also be equivalently formulated in the time domain, i.e. in terms of point-charge wake functions or finite-length bunch wake potentials, which could be useful for cross-checking EM field solver code results.

For the optical impedance of the iris, the right- and left-hand sides of Eq. (46) are plotted in Fig. 12 vs. the reference orbit offset for three representative values of parameter δ. Both sides are clearly equal to within the plot resolution.

D. Frequency range

We conclude by discussing the frequency range applicability of the derived impedance formulas. First, we focus on the case of a slowly tapered collimator, $\theta \ll 1$, which will be required to reduce the impedance at low frequencies. On top of that we concentrate on the practically relevant case of a relatively large, but not extreme, aperture variation, so that, by order of magnitude, $g \approx a \approx L_t\theta$, where g is the minimum collimator aperture, and L_t is the transition length, all introduced in Fig. 1. Depending on the length of the collimator middle section, denoted L_m, the applicability conditions of the optical model, reviewed at

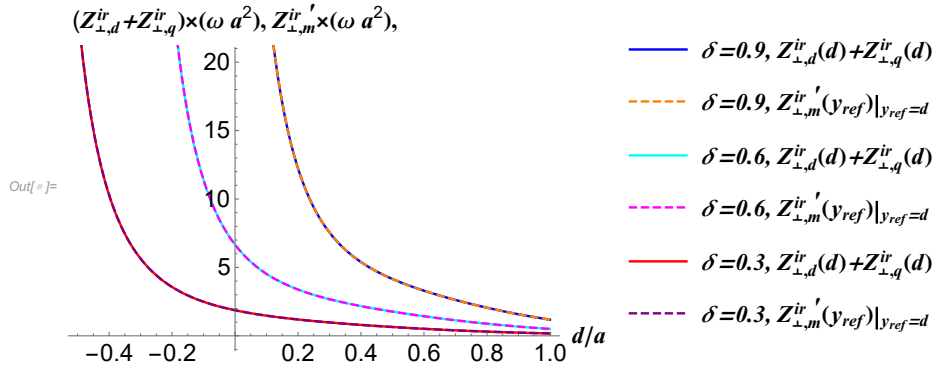

FIG. 12: Sum of the dipole and monopole impedance components for the iris (solid curves) and the derivative of the monopole component with respect to the offset of the reference trajectory (denoted by prime in the legend and the axis labels, dashed curves).

the beginning of Section II, reduce to

$$\omega/c \gg (g\theta)^{-1}, \quad L_m \lesssim L_t, \tag{47}$$

$$\omega/c \gg \frac{L_m}{L_t}(g\theta)^{-1}, \quad L_m \gg L_t. \tag{48}$$

Under these conditions the impedance of the collimator structure is given by the optical model due to the corresponding iris, Eqs. (24)-(27)

In addition, for the long collimator there is an intermediate range of high frequencies

$$(g\theta)^{-1} \ll \omega/c \ll \frac{L_m}{L_t}(g\theta)^{-1}, \quad L_m \gg L_t, \tag{49}$$

where the impedance is given by the sum of the respective optical models due to the step-up and step-down transitions, given by Eqs. (28)-(35).

For steeply-tapered or un-tapered collimators, the optical impedance model frequency range is also given by Eqs. (47)-(49), with replacements $\theta = 1$ and $L_t = g$. The actual optical model impedance formulas, are, of course, independent of the tapering angle.

V. CONCLUSIONS AND OUTLOOK

High frequency geometric impedances of a KEKB-style asymmetric collimator structure, Eqs. (24)-(27), were derived by applying the optical impedance formalism originally developed in [5, 6]. Impedance dependence on geometric parameters, such as the middle

collimator pipe offset $\Delta = \delta/a$ and the orbit offset in the incoming collimator pipe d, have been investigated. Divergences of the impedance components when the beam is close to the collimator pipe wall were characterized. On top of that, we found the individual optical model expressions for the impedances of the step-up and step-down structures, Eqs. (28)-(35). Summed up together, they give the intermediate frequency range optical model for long collimators, which, in turn, allows one to estimate the (weak) dependence of the collimator impedance on its length L_m. The impedance expressions for the step-up and step-down could also be useful by themselves, i.e. in code bench-marking, or in studies of other compound impedance-carrying structures.

The final impedance expressions are presented in the form of simple 1D integrals, which are easy to evaluate and analyze numerically. The numerical results, calculated for several representative parameter values, are listed at the end of sub-Section IV B. For example, for the nominal case of δ=0.6 and $d = 0$, the high frequency longitudinal impedance on the reference trajectory is $1.394/c$, corresponding to 41.5 Ohms in SI. This value agrees well with the simulations by ECHO, which is a 3D, time-domain finite-difference code [11]. Further illustration of the agreement of our analytical results with ECHO is given in the Appendix.

For this significantly asymmetric collimator we showed that for any reasonable off-axis displacement of particles, the transverse monopole impedance kick is very large compared to those of the dipole or quadruple impedance[5]. This kick, proportional to the total beam charge, varies with the particle position within a bunch, and could lead, among other things, to an emittance increase, as well as to the variation in closed orbits of the beam particles, resulting in beam size increase. Additional adverse effects may arise in the crab cavities. If strong enough, all of these effects could result in luminosity degradation. On the other hand, because the monopole kicks are independent of the transverse position of a particle, they do not directly contribute to beam instabilities. Further investigation will be required to understand the monopole (as well as other) impedance implications for the beam dynamics at the EIC ESR. As is clear from this note, a symmetric (in the collimation plane) collimator design alternative, would eliminate the monopole impedance when the beam orbit lies in the plane of symmetry, but it will increase the other three impedance components by a factor

[5] Strictly speaking this was only shown for high frequency impedance, implying very short bunches. However, from geometric considerations, we could argue that this statement is true for all frequency and bunch length ranges.

of two to four for the same stay-clear aperture. A fully axially symmetric design would, of course, eliminate the quadrupole impedance as well.

Apart from the optical model impedance expressions derived for the collimator, we pointed out a universal property of the monopole impedance for an arbitrary structure, Eq. (46), relating this impedance to the sum of the dipole and quadrupole impedances of the same structure. This property, or its time-domain counterpart, could be useful for cross-checking the results of EM field solver codes, or for other calculations.

The optical impedance model expressions, derived in this note, give the high frequency impedance asymptotics which are frequency-independent for the longitudinal case. By design, the optical model ignores diffraction effects, which, of course, are present in the asymmetric collimator structure and contribute to the impedance at lower frequencies. These effects result in the well-known diffraction model (i.e. [12]) which scales as $Z_\parallel \sim \omega^{-1/2}$. In the time domain both models result in point-charge wake functions which diverge at the location of the driving particle. Specifically, $W_\parallel^\delta(z \to 0^-) \sim \delta(z)$ and $W_\parallel^\delta(z \to 0^-) \sim |z|^{-1/2}$, for the optical and diffraction models respectively. With both divergent models subtracted, the rest of the wake function is well-behaved and it can be found from the wake potentials due to a relatively long Gaussian bunch, calculated by time-domain EM codes [3]. The total wake function is then found by adding back the optical and diffraction models. A similar approach also works to find the wake function in the transverse plane [4]. Finding the point-charge wake functions of the asymmetric collimator by this approach will be the subject of our future work.

VI. ACKNOWLEDGMENTS

I acknowledge insightful discussions about the intricacies of the optical impedance model with Karl Bane and Gennady Stupakov. I am grateful to Michael Blaskiewicz for critically reading this note, as well as to Alexei Blednykh, Medani Sangroula and Gang Wang for independently checking a fraction of the results with different time-domain EM field solvers.

---

[1] *Electron-Ion Collider eRHIC Pre-Conceptual Design Report*, Tech. Rep. BNL 205809-2018-FORE, v14, July 11 (BNL, 2019).

[2] Y. Suetsugu, Nuclear Instruments and Methods in Physics Research Section A: Accelerators, Spectrometers, Detectors and Associated Equipment, **513**, 465-472 (2003).

[3] B. Podobedov and G. Stupakov, Phys. Rev. ST Accel. Beams, **16**, 024401 (2013).

[4] B. Podobedov and G. Stupakov, Proceedings of PAC2013, WEODB1, 778 (2013).

[5] G. Stupakov, K. Bane, and I. Zagorodnov, Phys. Rev. ST Accel. Beams, **10**, 054401 (2007).

[6] K. Bane, G. Stupakov, and I. Zagorodnov, Phys. Rev. ST Accel. Beams, **10**, 074401 (2007).

[7] S. Heifets, A. Wagner, and B. Zotter, *Generalized Impedances and Wakes in Asymmetric Structures*, SLAC Report No. SLAC/AP110 (1998).

[8] S. A. Heifets and S. A. Kheifets, Rev. Mod. Phys., **63**, 631 (1990).

[9] E. Gianfelice and L. Palumbo, IEEE Trans. Nucl. Sci., **37**, 1084 (1990).

[10] I. Zagorodnov, K. Bane, Proceedings EPAC'06, 1081 (2006).

[11] I. Zagorodnov and T. Weiland, Phys. Rev. ST Accel. Beams, **8**, 042001 (2005).

[12] A. W. Chao, *Physics of Collective Beam Instabilities in High Energy Accelerators* (Wiley, New York, 1993).

APPENDIX A: COMPARISON TO ECHO SIMULATIONS

To cross-check some of our results, we performed a number of ECHO simulations. For all the cases we looked at so far, we generally found very good agreement, as long as the bunch was short enough for the optical regime to apply, see sub-Section IV D. To properly choose the mesh size for a given bunch length, as well as for the iris thickness (taken to be one mesh size thick), we followed the guidance in [6], sub-Section II A. Finally, to extract the normalized optical model impedance values from the ECHO simulation results we used the following expressions, expected to hold in the optical regime,

$$Z_{\parallel} \times c = \frac{4\,\pi}{Z_0\,c}\; 2\sqrt{\pi}\,\sigma\,k_{\parallel}, \tag{A1}$$

$$Z_{\perp,m} \times (\omega a) = \frac{4\,\pi}{Z_0\,c}\; 2\,a\,k_{\perp,m}, \tag{A2}$$

$$Z_{\perp,d} \times (\omega a^2) = \frac{4\,\pi}{Z_0\,c}\; 2\,a^2\,k_{\perp,d}, \tag{A3}$$

$$Z_{\perp,q} \times (\omega a^2) = \frac{4\,\pi}{Z_0\,c}\; 2\,a^2\,k_{\perp,q}, \tag{A4}$$

where σ is the rms length of the Gaussian bunch used in the simulation, $k_{\parallel}$ is the loss factor, $k_{\perp,m}$, $k_{\perp,d}$, and $k_{\perp,q}$ are the transverse kick factors, obtained by integrating the corresponding

wake potentials, calculated by ECHO, weighted by the longitudinal charge density.

As an illustration, in Fig. 13 we plot our analytical result for the longitudinal impedance of the iris as a function of parameter δ together with the corresponding results from ECHO, post-processed using Eq. (A1). ECHO calculations were performed for the iris structure shown in Fig. 3 with the pipe radius of a=1 cm, using equal mesh sizes of 0.1 mm in the longitudinal and both transverse directions. The rms bunch length used in the simulations for the results plotted in the figure was 0.5 mm.

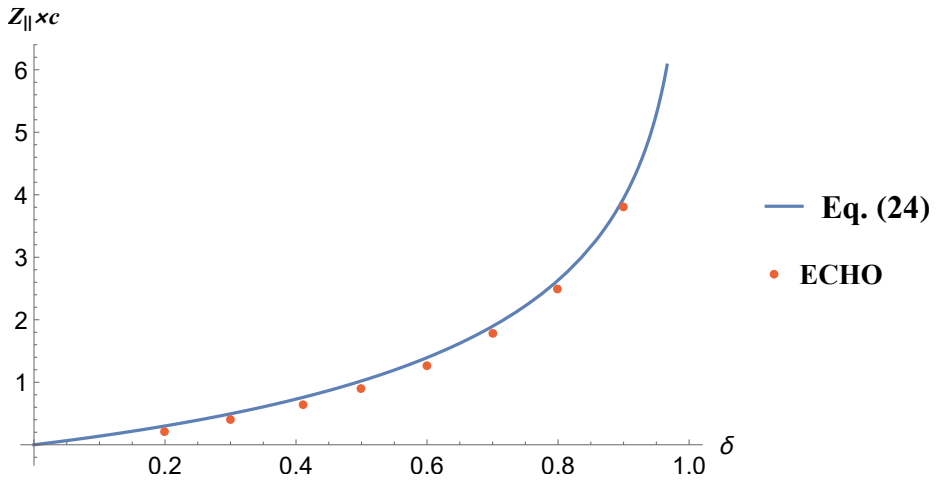

FIG. 13: Analytical and numerical results for the longitudinal impedance of the iris.

Clearly, for these parameters the ECHO simulations and the analytical result agree well, at the ten percent level or better, depending on the value of δ. Furthermore, as we checked separately for a subset of cases, the agreement becomes even better, if an even shorter bunch is used in the simulations, so that we move further into the optical regime. For instance, at $\delta = 0.6$ the ECHO result in the figure is 0.911 of the analytical value. When the bunch length is halved to σ=0.25 mm, the ECHO result goes to 0.954 of Eq. (24).